Rock Mechanics and Rock Engineering (2022) 55:3279–3300
https://doi.org/10.1007/s00603-022-02795-x

ORIGINAL PAPER

Influence of Block form on the Shear Behaviour of Soft Soil–Rock Mixtures by 3D Block Modelling Approaches

Han Zhang[1,2] · Daniela Boldini[3] · Lehua Wang[1,2] · Huafeng Deng[1,2] · Chang Liu[4]

Received: 26 July 2021 / Accepted: 27 December 2021 / Published online: 15 February 2022

Abstract
The influence of block forms on the shear behaviour of soil–rock mixtures with soft blocks (soft S–RMs) can be efficiently investigated by the discrete element method (DEM) on the basis of accurate 3D models accounting for the block breakage. This paper proposes a novel modelling approach, based on the spherical harmonics series, for the generation of 3D block geometries with different forms but same convexity and angularity. An already existing non-overlapping modelling approach was improved, characterized by a reduced computational cost, for the set-up of 3D block DEM models accounting for the block breakage. A number of soft S–RM DEM samples, subjected to numerical direct shear tests, were generated to analyze the influence of block forms and volumetric block proportion *VBP* on the mesoscopic and macroscopic behaviours. The results showed that the breakage degree is maximum for the spheroidal blocks, followed by the oblate, prolate and blade ones, due to the combined influence of the block frictional sliding and rotation. The shear strength of soft S–RMs is mainly controlled by the block interlocking and breakage, being maximum in the case of spheroidal block samples when the applied normal stress is low and in the case of prolate and blade ones for a high normal stress. It was found that a nonlinear Mohr–Coulomb criterion can provide a good description of the shear strength envelope of soft S–RMs. Soft S–RMs are characterized by a higher friction angle if composed by spheroidal and prolate blocks when the *VBP* is 40%, due to their elevated block interlocking, and in the case of prolate and blade blocks when the *VBP* is 60% at the higher normal stress, due to their lower block breakage degree.

Highlights

- A spherical harmonics based approach was proposed for generating 3D block geometries with different formsbut same convexity and angularity.
- A non-overlapping approach was improved for set up of 3D block DEM models considering the possible block-breakage with a reduced computational cost.
- The influence of block form on the meso- and macro-shear behaviours of soft S-RM were analyzed.
- Block form has great influence of the shear behaviour of soft S-RMs, especially when the value of *VBP* is high.

✉ Daniela Boldini
daniela.boldini@uniroma1.it

1 Hubei Key Laboratory of Disaster Prevention and Mitigation, China Three Gorges University, Yichang 443002, China

2 College of Civil Engineering and Architecture, China Three Gorges University, Yichang 443002, China

3 Department of Chemical Engineering Materials Environment, Sapienza University of Rome, Via Eudossiana 18, 00184 Rome, Italy

4 Faculty of Engineering, China University of Geosciences, Wuhan 430074, China

Keywords Soft S–RM · Block form · 3D block geometry modelling · 3D block DEM modelling · Mesoscopic shear behaviour · Macroscopic shear behaviour

List of symbols

EI	Elongation
FI	Flatness
C_V	Convexity
R	Roundness
l_a, l_b, l_c	Long, intermediate and short axis dimension of a block
$r_{\min}$	Minimum curvature radius of a vertex
r_{ins}	The radius of the maximum inscribed sphere of a block particle
N_V	The number of vertices on the block surface
N_c	The number of corners on the block surface
a_n^m	SH coefficients
n	SH degree
m	SH order
E_f, E_r and E_c	Relative errors of form descriptors, roundness and convexity of SH blocks
N_f, N_a and N_c	n threshold values of form, angularity and convexity
$\overline{a_n^m}$	Normalisation SH coefficient
$a_n^{\prime m}$	Random SH coefficient with n degree
r	Random number
r_a	Ratio of the maximum sphere diameter to the block particle size
r_b	The ratio of the maximum sphere diameter to the minimum one
N	Number of generated balls in a block DEM model
VBP	Volumetric block proportion
N_{block}	Total number of blocks in an S–RM sample
B_N	The number of balls in a block in contact with the balls belonging to other blocks
B_P	Average percentage of balls in a block contacting with the balls belonging to adjacent blocks
E_μ	Accumulated energy dissipate
σ_n	Normal stress
R_a	Average accumulated rotation magnitude
$N_{\text{non-break}}$	The number of balls still bonding with the other balls in the block
r^{ball}	The rotation magnitude of a ball
B_r	Meso-ratio of block breakage
$N_{\text{bond-break}}$	The number of broken bonding
N_{bond}	The number of bonding contacts before the shearing
φ	Friction angle
c	Cohesion
φ_0	Initial friction angle
$\Delta\varphi$	The φ reduction magnitude with increasing σ_n

1 Introduction

Soil–rock mixtures (S–RMs) are extremely inhomogeneous geomaterials typically composed of rock blocks with various sizes and a fine-grained soil matrix (Xu 2008). They are widespread worldwidely over natural slopes (Medley 1994; Li et al. 2004; Sonmez et al. 2006; Coli et al. 2011; Minuto and Morandi 2015; Napoli et al. 2021) and are also used as construction materials in embankments and fills (Calseira and Brito 2014; Zhang et al. 2016a, b; Cen et al. 2017). To assess the stability of such natural and artificial geostructures, several researches have investigated the S–RM shear response, showing that the shear strength of S–RMs is mainly controlled by the volumetric block proportion (*VBP*) (Medley and Rehermann 2004; Xu et al. 2011; Kalender et al. 2014; Napoli et al. 2018a, b, 2019), but is also affected by the moisture content (Xu et al. 2007; Li et al. 2020), block grain size distribution (Hamidi et al. 2012; Zhang et al. 2016a, b), block size (He et al. 2020; Christoph et al. 2021) and block orientation (Lindquist 1994; Khorasani et al. 2019). In addition, for the block shape, Graziani et al. (2012) found that the friction angle of S–RM is higher when the blocks are triangular, followed by rectangular and then prismatic blocks. Li et al. (2013) suggested that the friction angle of clay–gravel mixtures increases with the increase of convexity of gravel particles and decreases with their elongation. Jin et al. (2017a) pointed out that the strength of S–RMs with angular crushed blocks are higher than those occurring in the case of smooth cobbles. Wang et al. (2020a, b) showed that the shear strength increases when the block concavity is higher, possibly in relation to the more elevated number of contacts among blocks. All these studies demonstrated that the block shape also has a large influence on the shear mechanical properties of S–RMs.

According to the Chinese Standard (GB 50218-94), a rock is defined as a "soft rock" when its uniaxial compressive strength is lower than 30 MPa; otherwise it is considered as a "stiff rock". The aforementioned researches are all focused on the behaviour of S–RMs containing stiff rock blocks, called as "stiff S–RMs", characterized by blocks difficult to be broken during shearing. However, S–RMs with soft rock blocks, referred to as "soft S–RMs" in this paper, also exist and were found in landslides and artificial fills (Roadifer and Forrest 2012; Kahraman et al. 2015; Liu et al. 2020; Zhang et al. 2020; Xu and Zhang 2021). In this case, the soft blocks can easily break during shearing processes, implying a shear behaviour is completely different from that of the stiff S–RMs. Roadifer and Forrest (2012) and Hu et al. (2018) both found that the friction angle and cohesion of soft S–RMs increase with the increase of *VBP* in the range 20–60%, differing from the response of stiff S–RMs. Zhang et al. (2020) and Hu et al. (2021) indicated that for similar values of *VBP*, the friction angle of soft S–RMs is smaller than that of stiff ones, while the cohesion is higher. Liu et al. (2017) found that the blocks are easier to break with the decrease in moisture content, while both the cohesion and the friction angle decrease with it. Xu and Zhang (2021) found that the shear response of specimens prepared using the equal quantity substitution method, that consists in replacing the oversize particles with smaller particles having an equal weight, is more similar to that of natural gradation samples if compared to the similar gradation method, in which the oversize particles are replaced on the basis of a parallel gradation curve. Liu et al. (2017), Wei et al. (2018) and Tu et al. (2021) all pointed out that the shear strength envelope of soft S–RMs is non-linear, this tendency being more manifest with the increase in the block breakage degree during the shearing process. In summary, it can be synthesized that the shear behaviour of soft S–RMs under different *VBP*, moisture content, sample size and gradation has been investigated in the last years, without, however, considering the influence of the block shape.

The effect of the block shape on the shear behaviour of soft S–RMs can be straightforwardly analyzed by numerical tests considering various block shapes, while the use of laboratory tests would be extremely complicated. As such, the set-up of soft S–RMs models accounting for an accurate 3D block shape is very significant. 3D numerical models for representing the real structure of S–RMs have been also recently developed. Coli et al. (2012) and Xu et al. (2016) simplified the block geometry by adopting ellipsoids and octahedrons. Jin et al. (2017b) proposed a method for creating random blocks having the same dimension of the real ones but a random convexity. Wang et al. (2020a, b) considered an approach for creating random convex polyhedron blocks by extending the edges of hexahedron geometries. Meng et al. (2020) presented a novel 3D S–RM modelling method for the generation of random concave polyhedrons representing the blocks. Nevertheless, the geometries of the random convex or concave polyhedrons are still simplifying most of the surface details of real blocks, characterized by different morphological features. To overcome this limit, a 3D modelling approach was proposed for the generation of a large number of random soft blocks having the same morphological features of the real blocks. The approach followed by Hu et al. (2021) was based on spherical harmonic (SH) series applied to the images of blocks scanned by the X-ray tomography (CT). However, it should be stressed that a block model, characterized by specified morphological parameters, cannot be set-up by this method, because of the randomness of the morphology of generated blocks. Accordingly, it is not possible to analyze the influence of a single morphological feature, such as the form, by contemporary eliminating the influences of the others, such as the convexity and angularity.

In this study, a mathematical approach for the generation of 3D S–RM models with specified morphological features for DEM simulations is proposed. Reference is made to a case-history already investigated by the authors, i.e. the construction of an electronic converter station in the Yunnan Province (China), characterized by the use of soft S–RMs as a filling material in artificial slopes (Hu et al. 2021). A limited number (e.g. 350) of highly weathered shale blocks in the S–RM were reconstructed by CT technology and image processing. To investigate the influence of block forms (e.g. spheroidal, oblate, prolate and blade) on the shear behaviour, eliminating the effect of other morphological features, a 3D modelling approach, characterized by block geometries with different forms but same convexity and angularity, was developed on the basis of SH series of the CT scanned blocks. An improved non-overlapping combination approach was also adopted for generating 3D block DEM models with a reduced computational time and accounting for the possible block breakage. Soft S–RMs models with four different block forms and two *VBP*, namely 40% and 60%, were thus generated and their response during direct shear test simulations was analyzed in detail.

2 CT Reconstruction and Form Characteristics of Shale Blocks in S–RM

2.1 CT Reconstruction of Shale Blocks

The reference soft S–RMs was adopted as a filling material for the construction of a 22 m-high artificial slope located in an electronic converter station in southwestern China. It is composed of a sandy silt matrix and strong-weathered argillaceous shale blocks (Fig. 1), characterized by an uniaxial compressive strength of 4.3 ± 1.5 MPa determined by means of point load tests (Zhang et al. 2020). The shear mechanical properties of this material were investigated by performing some large-scale direct shear tests (DSTs) with a cylindrical shear box 400 mm in height and 560 mm in diameter. The laboratory direct shear tests were performed at the following values of the applied normal stress: 100 kPa, 200 kPa, 400 kPa and 500 kPa. The maximum particle size of shale blocks in the DSTs was

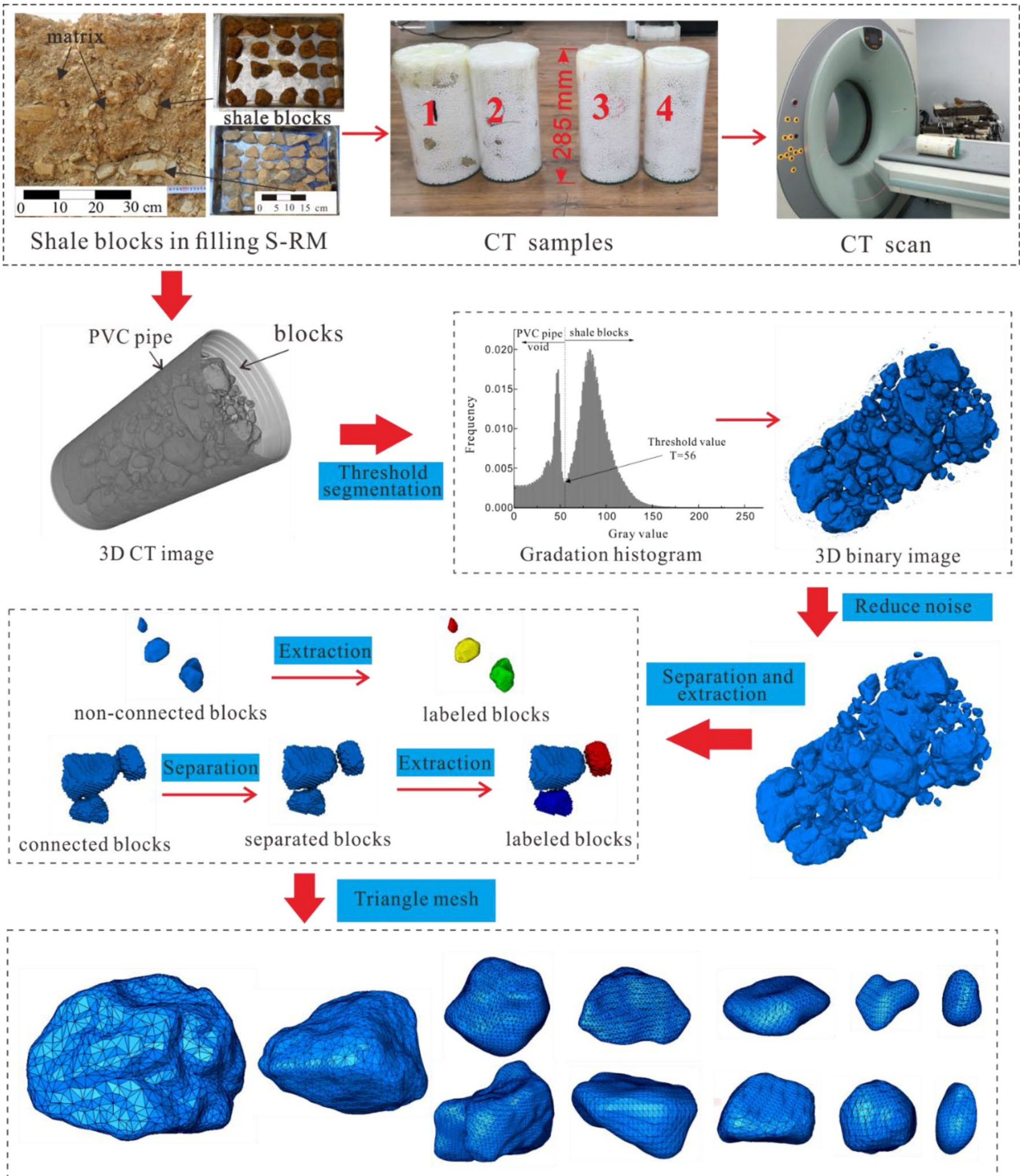

Fig. 1 CT scan of the shale blocks and 3D image processing

80 mm, and the *VBP* of the tested samples were 35–60%. After the DSTs, the CT technique was applied to reconstruct the 3D block geometries, as described in detail in Hu et al. (2021). Four CT samples with 145 mm diameter and 285 mm height, containing about 350 blocks were prepared for the scanning by the Siemens Somatom Sensation 40 CT system. Image processing was implemented for reconstructing the block geometries, as summarized in Fig. 1. The process includes threshold segmentation, 3D median filter, 3D connected components' extraction and watershed-based segmentation. More specifically, the function *Separate Object* in AVIZO, a 3D combination method of watershed, distance transform and numerical reconstruction algorithms, was employed to separate and extract the blocks connected with each other. Finally, all

block surfaces were meshed with triangles using the function *Generate Surface* in AVIZO.

2.2 3D Blocks' Morphology Quantification

The 3D morphology of particles can be expressed in terms of form, convexity and angularity, usually measured by the following descriptors (Nie et al. 2020): two aspect ratios of principal dimensions, i.e. elongation index *EI* and the flatness index *FI*, sphericity, convexity C_V and roundness R. *EI*, *FI* and sphericity are commonly used to describe the particle form, while R is used to quantify the particle angularity (Zhao and Wang 2016).

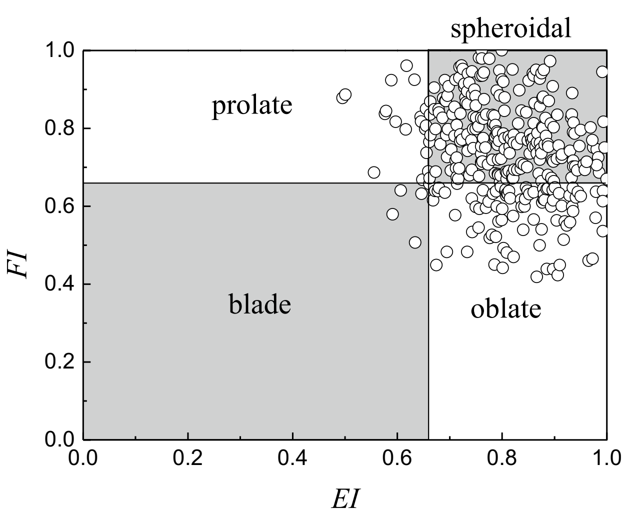

Fig. 2 Form characteristics of the CT scanned shale blocks

EI and *FI* are determined from the 3D principal dimensions of particles, consisting in the long l_a, intermediate l_b and short l_c axis dimension, with $EI = l_b/l_a$ and $FI = l_c/l_b$. Contextually, the intermediate dimension l_b is considered as the particle size of block. In the following, *EI* and *FI* will be used for describing the block form.

R is a parameter can be determined by the curvature of the particle surface corners as follows:

$$R = \frac{\sum_{i=1}^{Nv} g_i(\kappa) r^i_{\min}}{N_c r_{\text{ins}}}, \tag{1}$$

where $r^i_{\min}$ is the minimum curvature radius of the ith vertex, $r_{\min} = |\kappa_{\max}|^{-1}$. N_V and N_c are the number of vertices and corners on the block surface; r_{ins} is the radius of the maximum inscribed sphere of the block particle; $g(\kappa)$ is the corner judgment function. If the ith vertex is a corner, the function value is equal to 1; otherwise it is 0, expressed as follows:

$$g(\kappa) = \begin{Bmatrix} 1 & \text{if } r_{\min} < r_{\text{ins}} \\ 0 & \text{if } r_{\max} \geq r_{\text{ins}} \end{Bmatrix}. \tag{2}$$

The lower the R of a particle, the higher its angularity.

C_V represents how closely a particle resembles its convex hull, calculated by the particle volume V and the volume of its convex hull V_C, $C_V = V/V_C$. The convex hull is the smallest convex surface which contains all vertices of the original particle and can be obtained by the intrinsic function *convhull* in the MATLAB software. The C_V value of a particle lies in the range of [0, 1]: the lower the C_V of a block, the higher its concave and convex degree.

The block form can be defined as belonging to one of the following four categories on the basis of the

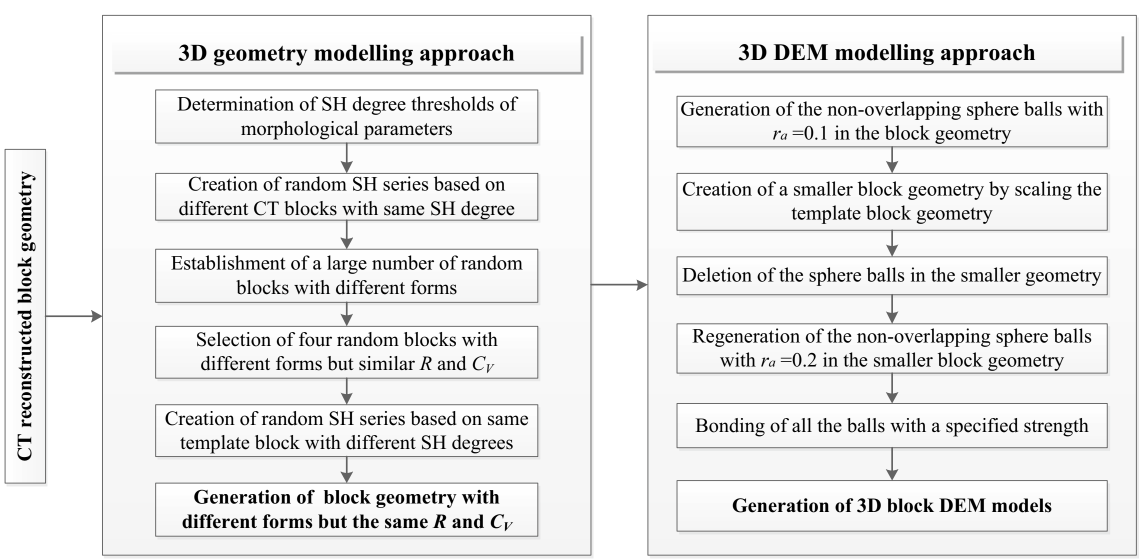

Fig. 3 Flowchart of 3D block modelling approaches

dimensional aspect ratios *EI* and *FI* (Zingg 1935): spheroidal (both *EI* and *FI* are larger than 2/3), oblate ($EI > 2/3$ while $FI < 2/3$), prolate ($EI < 2/3$ while $FI > 2/3$) and blade (both *EI* and *FI* are smaller than 2/3). The 3D principal dimensions of blocks were identified by rotating the principal axes according to the principal component analysis of the particle vertices. The single block was rotated, using the software MATLAB, until the long, intermediate and short axes were parallel to the *z*, *y* and *x* axes, respectively. Consequently, the principal dimension values l_a, l_b and l_c were easily obtained by measuring the block *x*, *y* and *z* dimensions in the rotated configuration. As shown in Fig. 2, the scanned shale blocks are mostly spheroidal and only subordinately oblate, with a few prolate and blade cases. More specifically, there were only 18 prolate and 4 blade blocks over the total 350 scanned ones.

3 Developed 3D Blocks Modelling Approaches

In order to analyze the influence of the block form on the shear behaviour of soft S–RMs, the effect of block convexity and angularity should be eliminated from the 3D model generation. However, due to the limited number of CT scanned shale blocks, especially those having a prolate or blade form, the request is rather difficult to be satisfied.

A novel 3D modelling approach was specifically proposed for generating block geometries, using spherical harmonics (SH) series of the CT scanned blocks, with different forms but the same *R* and C_V. In addition, an existing 3D DEM modelling approach, considering the possible breakage of blocks and correctly reproducing their morphology, was improved to reduce the calculation cost by limiting the number of bonding non-overlapping sphere balls. The flowchart of the two modelling approaches is shown in Fig. 3.

3.1 3D Block Geometry Modelling Approach

3.1.1 SH Function and Degree

SH analysis of a particle is commonly used for 3D analysis of the particle morphology. A SH series can be expressed as follows:

$$r(\theta, \phi) = \sum_{n=0}^{\infty} \sum_{m=-n}^{n} a_n^m Y_n^m(\theta, \phi), \tag{3}$$

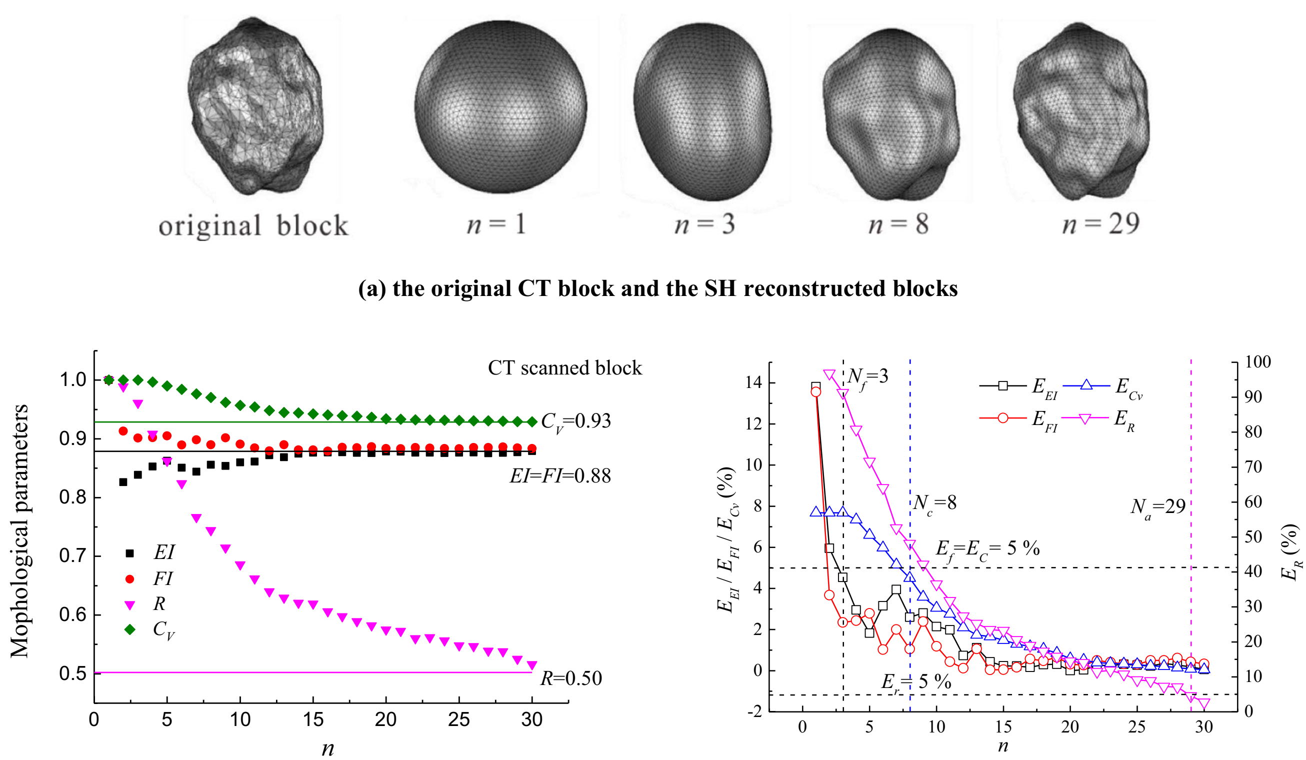

(a) the original CT block and the SH reconstructed blocks

(b) influence of *n* on the morphological features

(c) determination of *n* threshold values

Fig. 4 Influence of *n* on the morphological features of SH blocks and the determination of *n* threshold values where $r(\theta, \phi)$ is the polar radius from the particle centre to its surface vertices, with θ ranging in $[0, \pi]$ and ϕ in $[0, 2\pi]$. The a_n^m are the associated SH coefficients, the SH degree n and order m being respectively a non-negative integer from zero to infinity and an integer from $-n$ to n. $Y_n^m(\theta, \phi)$ is the SH function expressed by Eq. (4) that can be obtained by the associated Legendre function of Eq. (5):

$$Y_n^m(\theta, \phi) = \sqrt{\frac{(2n+1)(n-m)!}{4\pi(n+m)!}} P_n^m(\cos\theta) e^{\mathrm{i}m\phi}, \tag{4}$$

$$P_n^m(x) = \frac{(-1)^m}{2^n n!}(1-x^2)^{m/2} \frac{d^{n+m}}{dx^{n+m}}(x^2-1)^n. \tag{5}$$

3.1.2 Determination of SH Degree Thresholds of Morphological Features

The morphological features of the SH reconstructed blocks are affected by the adopted values of n (Zhou et al. 2015; Hu et al. 2021).

A CT block with a particle size of 41 mm was selected for the SH reconstruction with different n values, as shown in Fig. 4a. The relative errors of morphological features E are defined by comparing the morphological parameters of SH reconstructed blocks to those of the real CT ones. In particular, E_f, E_r and E_c are, respectively, the errors of form descriptors, roundness and convexity. These quantities were introduced to detect the minimum value of n necessary to accurately characterize the different morphological features of the blocks. For the balance of computational efficiency and morphology precision, a limit of 5% was considered for the relative error. The corresponding thresholds for the values of the required n are named N_f, N_a and N_c for the form, angularity and convexity, respectively.

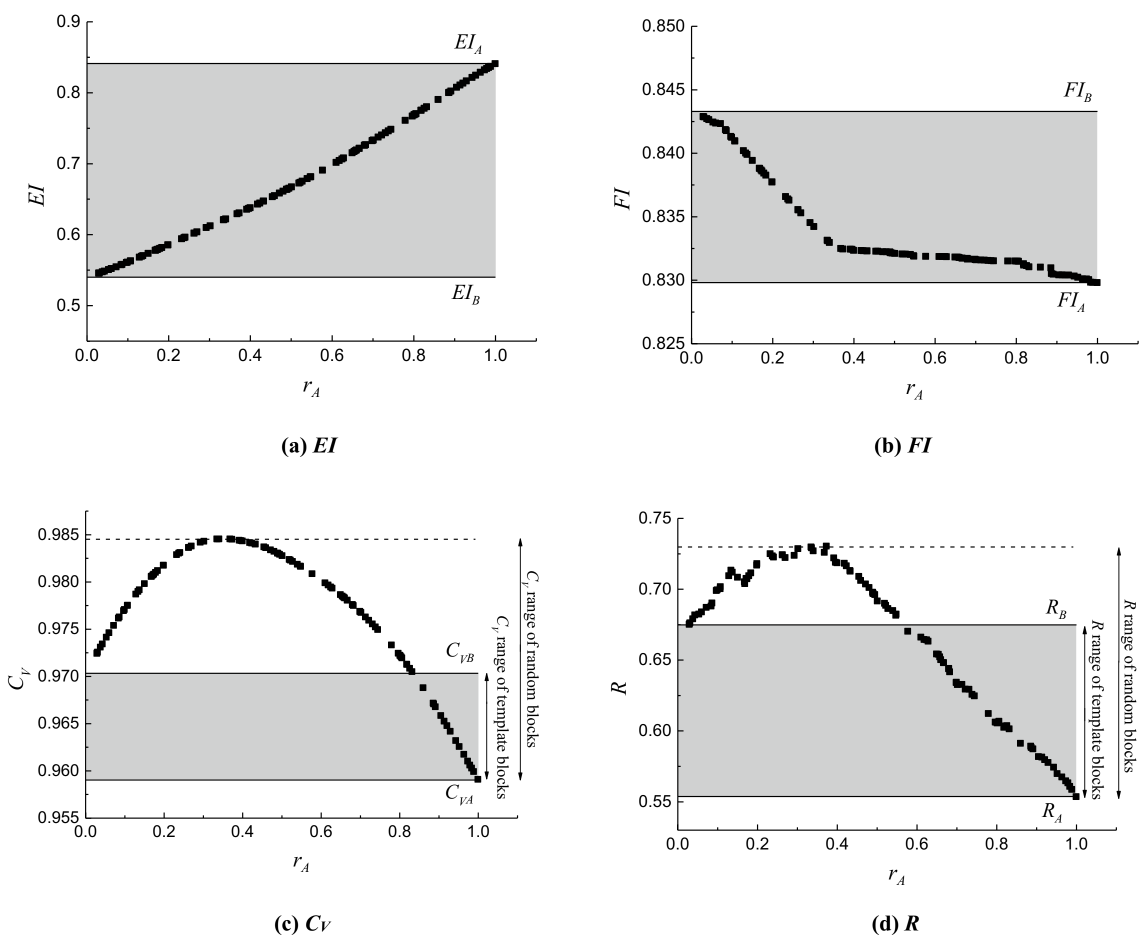

Fig. 5 Morphological features of the template and random blocks using generation approach with different blocks

The morphological parameters of the SH reconstructed blocks become closer to the CT ones with the increase of *n*. Except for the form parameter *EI*, the other descriptors all decrease with the increase of *n* (Fig. 4b). Significantly, the effect of the value of *n* on the *R* is much more relevant than for the other parameters, indicating that the angularity of blocks is more difficult to be characterized by SH series. Consequently, the N_f, N_c and N_a values are equal to 3, 8 and 29 (Fig. 4c).

3.1.3 Generation of a Large Number of Random Blocks with Different Forms

A large number of random blocks with different forms can be generated by creating random SH series on the basis of SH series of a limited number of different template blocks with the same *n*. For accurately characterizing all the morphological features, the SH series of CT blocks can be developed by considering the threshold N_a only, which was demonstrated to be typically much larger than N_c and N_f. Based on the N_a value, the normalisation SH coefficients of CT blocks, $\overline{a_n^m}$, can be obtained by first rotating the blocks to have their principal axes parallel to the global coordinate axes and then scaling their volume to unity.

The random SH coefficients $a_n'^m$ can be generated on the basis of a limited number of *M* template blocks by the following equation:

$$a_{N_a}'^m = \sum_{i=1}^{M} r_i \left(\overline{a_{N_a}^m}\right)_i, \ \sum_{i=1}^{M} r_i = 1, \tag{6}$$

where $a_{N_a}'^m$ are the generated random SH coefficients with N_a degree. r_i is a random number in the interval [0,1]. A set of *M* values of r_i can be randomly generated for creating a new random SH coefficient. As such, thousands of random blocks can be established when thousands of sets of random number are generated.

In the example of Fig. 5, 110 random blocks were generated on the basis of two template blocks A and B, r_A being the random number for block A and $r_B = 1 - r_A$ that for block B. It shows that even if the *EI* and *FI* values of generated random blocks are all in the range of those of the two

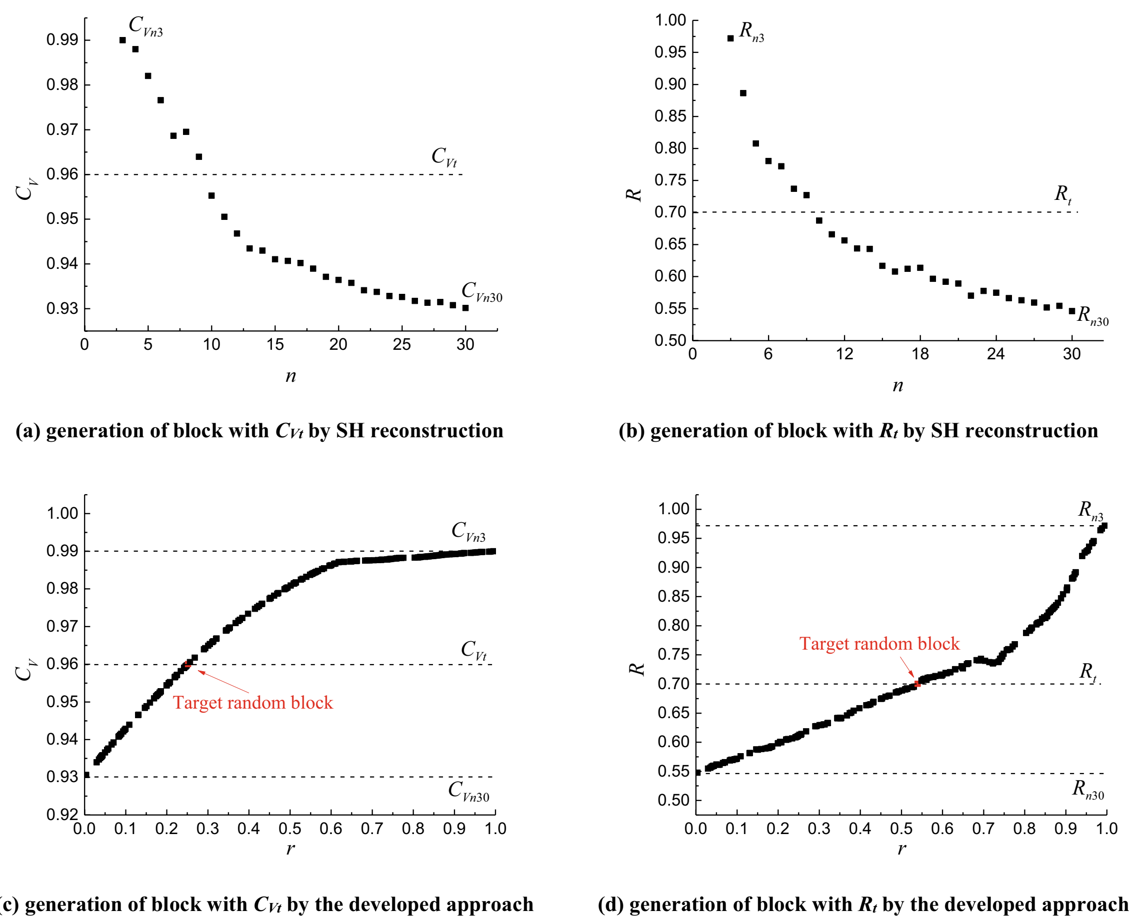

(a) generation of block with C_{Vt} by SH reconstruction

(b) generation of block with R_t by SH reconstruction

(c) generation of block with C_{Vt} by the developed approach

(d) generation of block with R_t by the developed approach

Fig. 6 Creation of a block with target C_V or *R* using SH reconstruction and the developed random generation approach

Table 1 First random generation

Template blocks	B1	B2	B3	B4
Form of template blocks	Spheroidal	Prolate	Oblate	Blade
C_V of template blocks	C_{V1}	C_{V2}	C_{V3}	C_{V4}
R of template blocks	R_{B1}	R_{B2}	R_{B3}	R_{B4}
Generated blocks	C1	C2	C3	C4
Form of generated blocks	Spheroidal	Prolate	Oblate	Blade
C_V of generated blocks	$C_{V\max}$	$C_{V\max}$	$C_{V\max}$	$C_{V\max}$
R of generated blocks	R_{C1}	R_{C2}	R_{C3}	R_{C4}

Where the $C_{V\max} = \max(C_{V1}, C_{V2}, C_{V3}, C_{V4})$

Table 2 Second random generation

Template blocks	C1	C2	C3	C4
Generated blocks	D1	D2	D3	D4
Form of generated blocks	Spheroidal	Prolate	Oblate	Blade
C_V of generated blocks	$C_{V\max}$	$C_{V\max}$	$C_{V\max}$	$C_{V\max}$
R of generated blocks	$R_{\max}$	$R_{\max}$	$R_{\max}$	$R_{\max}$

Where the $R_{\max} = \max(R_{C1}, R_{C2}, R_{C3}, R_{C4})$

template blocks, the C_V and R ones are not (Fig. 5). This evidence indicates that the proposed block generation approach can be used to create random blocks having a form variable in the same range of the template blocks but angularity and roughness parameters outside the corresponding ranges, as requested by the research target.

3.1.4 Generation of Random Blocks with Same Angularity and Roughness

Given a template block, a SH block with smaller C_V and R can be generated by simply reducing the value of n during the SH reconstruction. To exactly control the resulting values of C_V and R, a novel generation approach was developed described by Eq. (7):

$$a'^m_{n_2} = ra^m_{n_1} + (1 - r)a^m_{n_2}, \tag{7}$$

where $a'^m_{n_2}$ is the generated random SH coefficient for creating the random SH blocks, while the $a^m_{n_1}$ and $a^m_{n_2}$ are, respectively, the SH coefficients of the template block with n_1 and n_2 degree, with n_2 larger than n_1. r is a number generated randomly in the range of 0–1.

As an example, a template block with C_V of 0.93 and R of 0.55 was selected, fixing n_1 to 3 and n_2 to 30. For creating a block with target values $C_{Vt} = 0.96$ and $R_t = 0.70$, 28 SH reconstructed blocks were generated only by varying n from n_1 to n_2 (Fig. 6a and b). They are compared to the 200 random blocks created by the developed approach on the basis of Eq. (7) (Fig. 6c and d). Inspection of the figure reveals that the target values of C_{Vt} or R_t can be obtained by the developed approach, while not using the method by simply reducing the n, due to larger number of random blocks with different C_V and R can be generated by the improved approach.

Four blocks with different forms but similar C_V and R were selected from the large number of generated random blocks in Sect. 3.1.3, labelled as B1, B2, B3 and B4. For n varying from N_c to N_a, C_V of SH blocks did not significantly modify while R changed in a large extent because N_c is lower than N_a. To take advantage of this fact, two sequential random generations were performed for obtaining the target blocks D1, D2, D3 and D4, as summarized in Tables 1 and 2. In the first step, random blocks with the same C_V were first generated, followed in the second step by the generation of random blocks with the same R.

In the first random generation, N_r and N_f thresholds were adopted for the block generation by Eq.(8), so as to ensure form parameters in the range identified by the template blocks. In the second random generation, N_a and N_c were adopted in combination with Eq.(9) to control the forms and convexity of the generated blocks. They are as follows:

$$a'^m_{N_r} = ra^m_{N_f} + (1 - r)a^m_{N_r}, \tag{8}$$

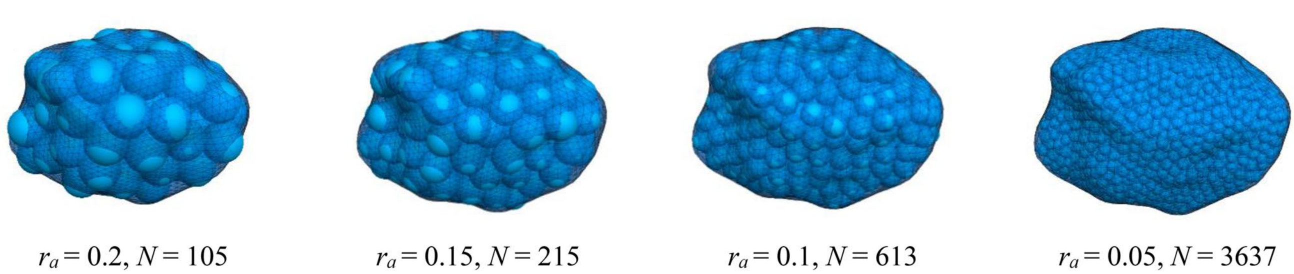

Fig. 7 DEM block models generated by the non-overlapping method using a different number of sphere balls

$$a''^{m}_{N_a} = ra^{m}_{N_r} + (1 - r)a^{m}_{N_a}, \tag{9}$$

where the $a'^{m}_{N_r}$ and $a''^{m}_{N_a}$ are the generated random SH coefficients in the first and second random generation, respectively, while $a^{m}_{N_f}$, $a^{m}_{N_r}$ and $a^{m}_{N_a}$ are the SH coefficients of the corresponding template blocks with N_f, N_c and N_a degree.

3.2 3D Blocks DEM Modelling Approach

After the geometry generation, a 3D DEM model was implemented by bonding the spherical balls to recreate the block geometry. In the following the commercial software PFC^{3D} was adopted.

3.2.1 Improved Non-Overlapping Modelling Approach

In general, two are the DEM modelling approaches used for reproducing the morphological features of irregular particles on the basis of a sphere assembly: (a) the non-overlapping combination method developed by Xu et al. (2016), with no or little overlapping being permitted between any pair of spherical balls; (b) the overlapping combination method proposed by Ai et al. (2011) and Ferellec and McDowell (2010), included as a built-in function in the code PFC^{3D}, allowing a large overlapping between two adjacent sphere balls. The overlapping method has been commonly used for the generation of unbreakable particles by neglecting the internal contact forces between the spheres, while the non-overlapping method has been preferred when the block breakage needs to be accounted for. As such, in this research the non-overlapping method was selected to generate the soft block DEM models.

In the traditional non-overlapping method, the number of generated balls N is mainly determined by the ratio of the maximum sphere diameter to the block particle size r_a and the ratio of the maximum sphere diameter to the minimum one r_b. Figure 7, as an example, shows DEM models obtained by setting r_b to 1.0 and changing r_a. It shows that the required value of N increases significantly with the reduction of r_a. In addition, when r_a is larger than 0.1, the angularity of the block is not well reproduced in the generated assembly, unless at least 600 balls are employed.

In order to save computational time, the non-overlapping method was improved by adopting a lower number of required spheres for the accurate description of block angularity. The adopted procedure can be summarized in the following steps (see also Fig. 8):

(a) a block DEM model with $r_a = 0.1$ and $r_b = 1.0$ was first established using traditional non-overlapping method, given by an assembly of 613 spheres (Fig. 8a);
(b) a smaller geometry characterized by particle size equal to the 80% of the template size was then generated by scaling down the template geometry based on the grav-

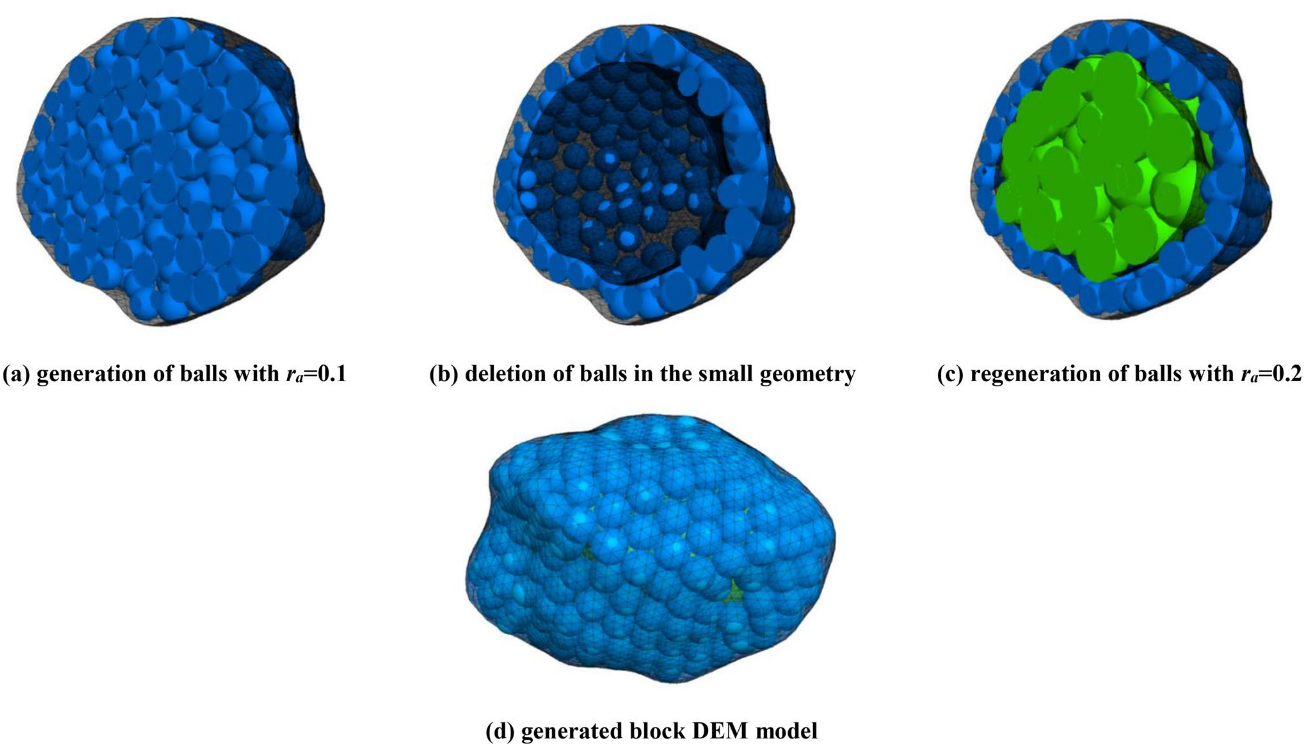

Fig. 8 Generation process of a block DEM model by the developed non-overlapping apporach

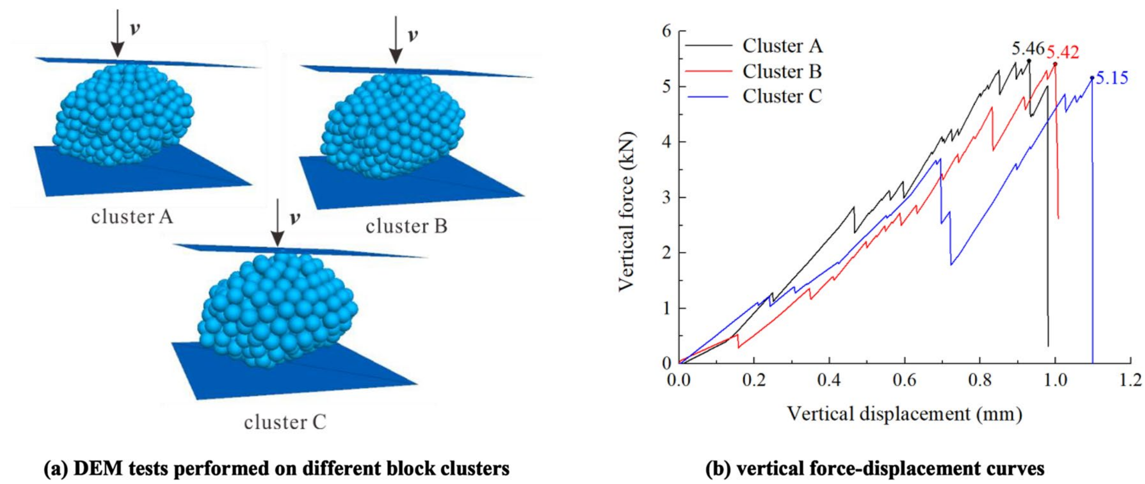

Fig. 9 Results of numerical unconfined compression tests on block clusters generated by different modelling approaches

Table 3 Morphological parameters of the generated random block geometries

Form of block geometry	*EI*	*FI*	C_V	*R*
Spheroidal	0.85	0.88	0.60	0.94
Prolate	0.56	0.82	0.60	0.94
Oblate	0.90	0.55	0.60	0.94
Blade	0.58	0.57	0.60	0.94

ity center and importing it into the DEM model generated in the step (a). The sphere balls in the smaller geometry were all deleted thus reducing the number of balls (Fig. 8b);

(c) sphere balls with $r_a = 0.2$ and $r_b = 1.33$ were regenerated (i.e., the green balls in Fig. 8c) in the smaller geometry for filling the block DEM model;

(d) the block DEM model was finally created by bonding the generated ball assembly with a specified bond strength.

The established block DEM model shown in Fig. 8d contained only 307 sphere balls, half of the value of 613 that required by the traditional non-overlapping method.

3.2.2 Influence of the Improved Approach on the Mechanical Properties

In this paragraph, the effect of a reduction in the particle number, related to the improved modelling approach, is analyzed in terms of mechanical properties. Three block clusters with the same geometry were generated for the analysis. They are: clusters A, generated using the traditional over-lapping method with $r_a = 0.1$ and consisting of 613 particles (Fig. 8a); cluster B, generated using the improved method and having 307 particles (Fig. 8d); cluster C, generated using the traditional method with $r_a = 0.12$ and characterized by 305 particles. The particles in each block cluster were bonded using the parallel bond model in PFC adopting the same meso-parameters, i.e. friction coefficient equal to 0.65 and bond strength equal to 1.5 MPa.

Unconfined compression tests were simulated by applying a vertical displacement rate of 0.002 mm/s (Fig. 9a). As shown in Fig. 9b, the reduction in the particle number by half associated to the traditional method (block cluster C) produced a reduction in the strength, the maximum vertical force decreasing from 5.46 to 5.15 kN. In contrast, almost comparable values of uniaxial compressive strength were obtained for the original cluster A and the cluster B with a reduced number of particles generated by the improved method.

It is therefore evident that the block DEM model generated by the improved modelling approach can reasonably reproduce the block morphology features and the block strength, by at the same time saving calculation cost.

4 Soft S-RM Models and DEM Tests

4.1 Establishment of Soft S–RM DEM Models

Four block geometries with different block forms were created by the novel proposed approaches. The morphological characteristics of the generated random blocks are listed in Table 3, in which the same value of convexity and roundness of the four blocks can be appreciated. Due to the limited computing capacity of the DEM software, only

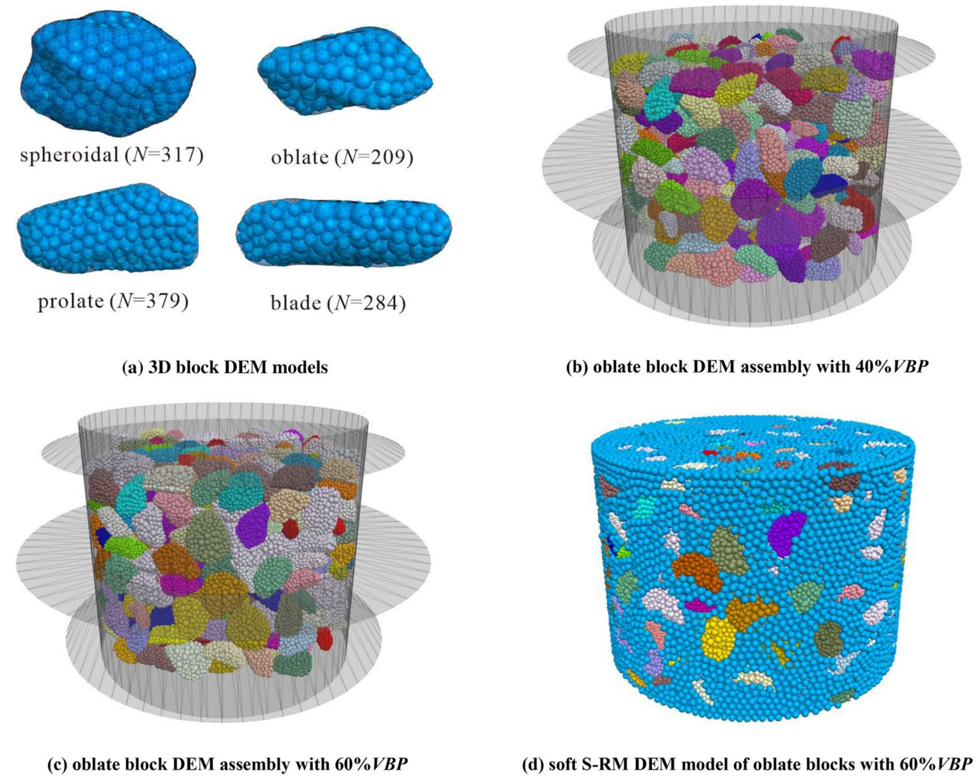

Fig. 10 Blocks and S–RM DEM models with different block forms and *VBP*

Table 4 Meso-parameters of materials used in S–RM models

Material	Contact model	Parameter	Value
Soil particles	Rolling resistant model	Density of particles (kg/m^3)	1850
		Damping factor of particles	0.2
		Elastic modulus of contacts (MPa)	10.0
		Poisson's ratio of contacts	0.5
		Friction coefficient	0.2
		Rolling resistance coefficient	0.05
Block particles	Parallel bond model	Density of particles (kg/m^3)	2500
		Damping factor of particles	0.2
		Elastic modulus of contacts (MPa)	110.0
		Poisson's ratio of contacts	0.5
		Friction coefficient	0.5
		Bond tensile strength (MPa)	1.04
		Bond shear strength (MPa)	1.04
Soil—block contacts	Rolling resistant model	Elastic modulus of contacts (MPa)	110.0
		Poisson's ratio of contacts	0.5
		Friction coefficient	0.35
		Rolling resistance coefficient	0.05
Block—block contacts	Rolling resistant model	Elastic modulus of contacts (MPa)	110.0
		Poisson's ratio of contacts	0.5
		Friction coefficient	0.45
		Rolling resistance coefficient	0.05

block models with a particle size in the range 40–80 mm were considered in the S–RM models.

The soft S–RM DEM models were generated following the next three steps:

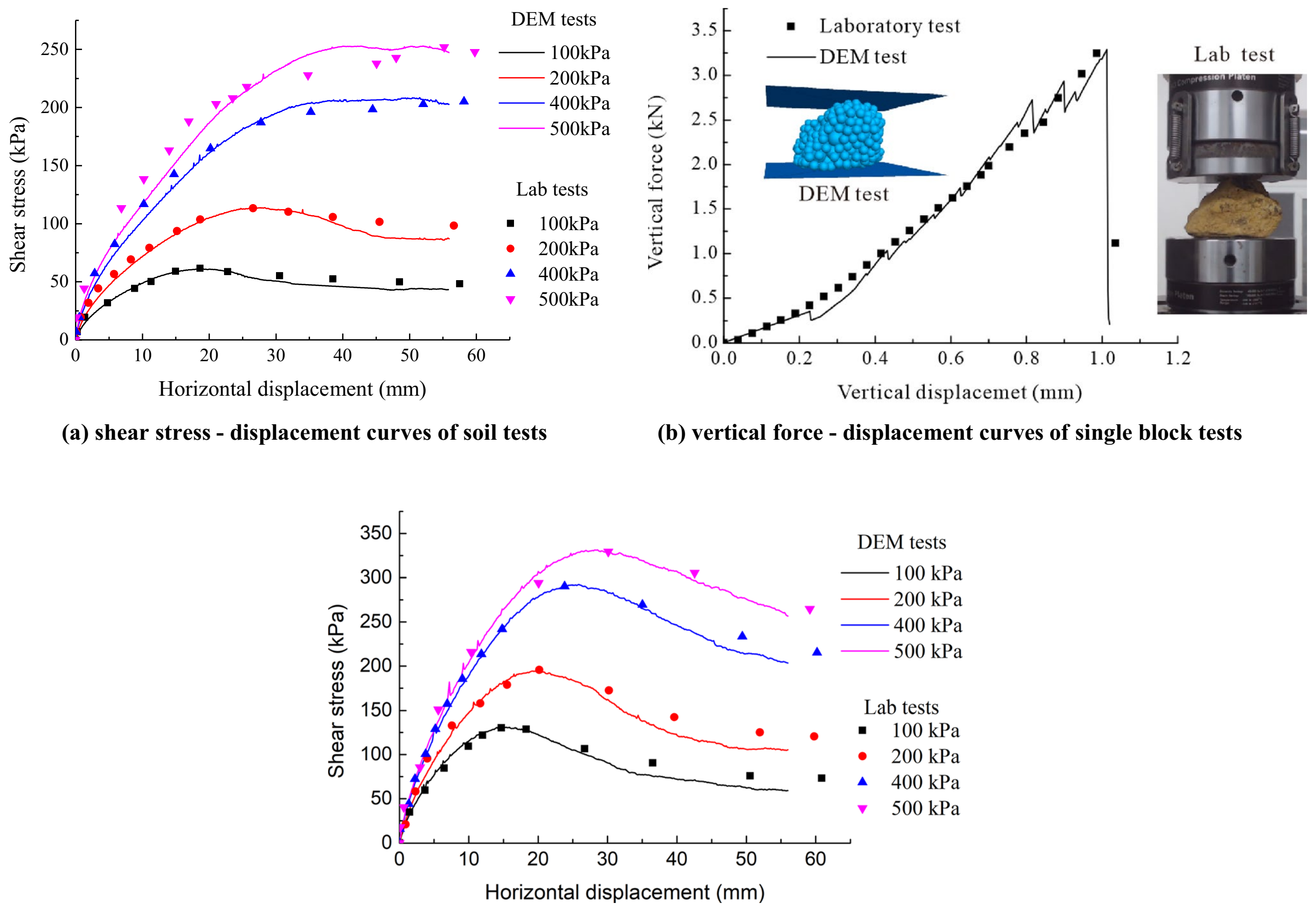

(a) shear stress - displacement curves of soil tests

(b) vertical force - displacement curves of single block tests

(c) shear stress - displacement curves of S-RM tests

Fig. 11 Calibration of meso-parameters of soft S-RMs

(a) The 3D block DEM models with different forms were created by adopting the developed DEM non-overlapping modelling approach, the number of sphere balls N used for representing the spheroidal, oblate, prolate and blade blocks was 317, 209, 379 and 284, respectively (Fig. 10a);

(b) The shear box employed in the laboratory tests mentioned in Sect. 2.1, a cylinder of a 560 mm in diameter and a 400 mm in height, was recreated by importing walls. For creating DEM assemblies with 40% and 60% *VBP* (see, for example, the oblate block DEM assembly in Fig. 10), block models with particle size of 40–80 mm were generated. More specifically, a percentage of 15%, 18%, 27% and 40% was considered respectively of the particle size groups 40–50 mm, 50–60 mm, 60–70 mm and 70–80 mm;

(c) Based on the soil/block threshold proposed by Medley (1994), particles with diameter lower than 10 mm can be considered as soil particles. To increase the computational efficiency, matrix balls in the DEM models were generated with a radius of 4.9 mm. The matrix porosity of DEM samples was set, by deleting or adding matrix balls, equal to 0.31 ± 0.005, a value in the range of that observed in the field (i.e. 0.28–0.36).

4.2 Determination of Meso-Parameters

In the S–RM DEM models, the rolling resistant model was adopted for representing the roughness of spherical soil particles. To reproduce the mechanical behaviour of breakable blocks, the parallel bond model was employed. The meso-parameters of matrix soil, blocks and contacts between soil-block and block-block were carefully calibrated using laboratory tests, as summarised in Table 4.

The matrix meso-parameters were calibrated against direct shear tests performed on the matrix soil, characterized by particle diameter lower than 10 mm and a 25% moisture content. The tests, carried out using a large shear box. The experimental and numerical shear stress—shear displacement curves show a good match (Fig. 11a), especially in terms of shear strength, demonstrating that the meso-parameters selected for the matrix can well reproduce its mechanical response in the DEM simulations.

One CT scanned block with a particle size of 55 mm was selected for performing an unconfined compression test with a vertical displacement rate of 0.002 mm/s. For the validation of the numerical procedure, the same test was simulated with a block cluster generated using the improved modelling approach. Some assumptions were made for the sake of simplicity, e.g. that the shear bond strength is equal to the tensile one, and the damping factor is equal to that of soil particles. The force–displacement curves shown in Fig. 11b indicate a good agreement between the numerical and experimental simulations, suggesting that the selected meso-parameters of block particles listed in Table 4 are suitable for reproducing the mechanical behaviour of the block.

The meso-parameters of contacts between soil-block and block-block were determined by calibrating a DEM S–RM model with 40% *VBP* against laboratory direct shear tests carried out on S–RMs having the same characteristics. In particular, the generation of blocks in the DEM models was based on the reconstruction of CT scanned blocks used in the lab tests. For the sake of simplicity, the rolling resistance coefficient of the two types of contacts was assumed to be the same, in consideration of the similar roughness of the soil and block spheroidal particles having similar radius in the DEM models. Inspection of Fig. 11c reveals that a very good agreement is reached between the shear stress—horizontal displacement curves of DEM and laboratory tests, especially up to the maximum strength. In the post-peak regime, the strength reduction is slighlty larger in the DEM tests, possibly because some block spherical fragments generated after the peak have a lower angularity than that of the real material, difficult to be avoided due to the limited computational capacity.

4.3 Numerical Direct Shear Tests

The applied normal stress and the size of S–RM sample used in the simulation are consistent with the lab tests introduced in Sect. 2.1. The shear loading was applied by setting a horizontal velocity of 0.2 mm/s to the upper portion of the shear box while fixing the lower one, slow enough to ensure a quasi-static equilibrium for the sample. The shear test was ended at a horizontal displacement of 56 mm, corresponding to 10% of shear strain.

During the shearing, not only the macro-mechanical properties, e.g. shear stress, normal stress, horizontal and vertical displacements, but also the meso-mechanical parameters, e.g. number of meso-cracks generated when the bond between block particles break, block rotation magnitude, number and the types of the particle contacts and the energy dissiption by the particle siding, were monitored and recorded automatically for investigating the effect of block forms on the shear behaviours of soft S–RMs.

5 Effect of Block Forms on the Shear Behaviours of Soft S-RMs

5.1 Mesoscopic Behaviour

5.1.1 Block Contact and Interlocking Characteristics

The internal structural characteristics of S–RM samples can be described by the amount of block contacts and interlock degree. In this research, the average percentage of balls in a block in contact with the balls belonging to adjacent blocks B_P was proposed for quantifying the structural characteristics of the S–RM:

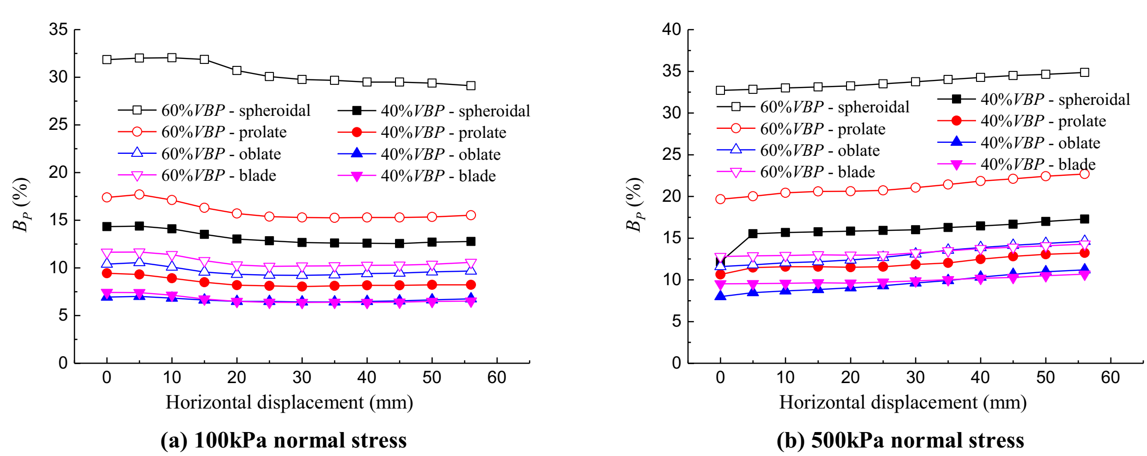

Fig. 12 Evolution of the percentage of block contacts B_P during the shearing stage of the direct shear tests for different block forms

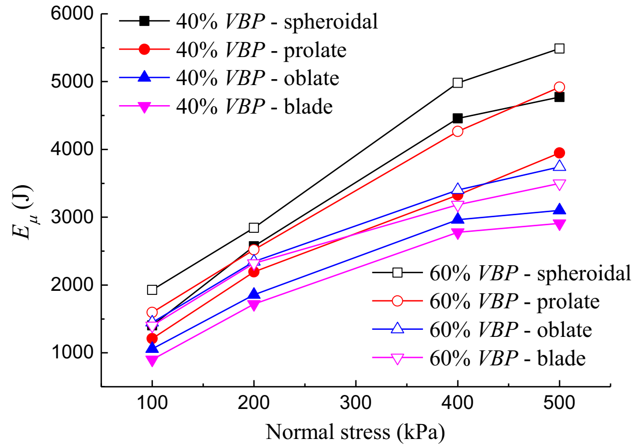

Fig. 13 Accumulated slip energy dissipation E_μ of soft S–RM samples when the horizontal displacement reaches 56 mm

$$B_P = \frac{B_N}{N_{\text{block}} \cdot N} \times 100\% , \tag{10}$$

where N_{block} is the total number of blocks in the S–RM sample; B_N is the number of balls in a single block in contact with the balls belonging to other blocks. The larger the B_P, the higher the block interlocking degree in the sample.

Four different types of ball contacts can be found in the S–RM sample, i.e. soil ball-soil ball, soil ball-block ball, block ball- block ball belonging to the block itself and block ball- block ball belonging to other blocks (B-OB). During the simulation, the B_N was obtained by calculated the number of contacts belonging to B-OB type.

Figure 12 shows the interlocking degree of blocks reduces slightly under the lower normal stress σ_n (i.e. 100 kPa), while becomes larger during the shearing stage under higher σ_n (i.e. 500 kPa). When the block form and σ_n are the same, the B_P values of samples with 60% *VBP* are obviously larger than those of samples with 40% *VBP*, demonstrating that the interlocking degree of blocks is larger for an higher *VBP*, as expected.

Inspection of the figure reveals that the B_P values is maximum for the spheroidal form, followed by the prolate form. The oblate and blade forms are characterized by similar and lower values. In addition, it is also evident that these differences are more pronounced for the higher *VBP*.

5.1.2 Particle Friction Characteristics

The particle frictional resistance is described by the accumulated energy dissipated by the particle frictional sliding E_μ. The calculated E_μ of all samples at the end of the shearing stage is summarized in Fig. 13, indicating that the larger values are found for the higher *VBP* and σ_n applied during the test.

The influence of block form is similar to that already observed for B_P. This circumstance demonstrates that the spheroidal blocks provide the largest frictional resistance in the S–RM sample, due to the likely higher frequency of contacts between balls, while that associated to oblate and blade blocks is limited.

5.1.3 Block Rotation Characteristics

The relative rotation of blocks is also an important parameter to describe the mesoscopic behaviour of S–RM samples. In this research, the average accumulated rotation magnitude R_a was proposed for evaluating the effect of block form and *VBP* on the block rotation:

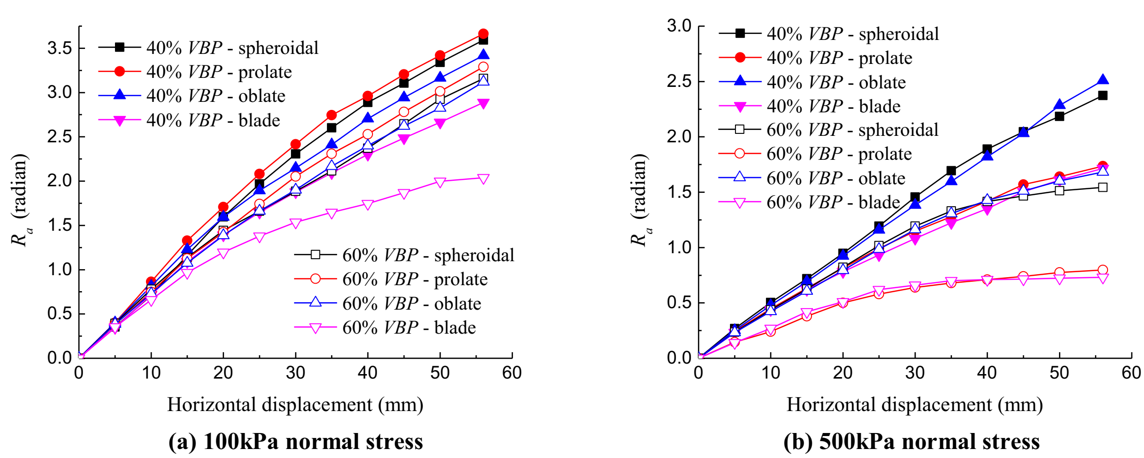

Fig. 14 Evolution of the average accumulated block rotation magnitude R_a during the shearing stage of the direct shear tests for different block forms

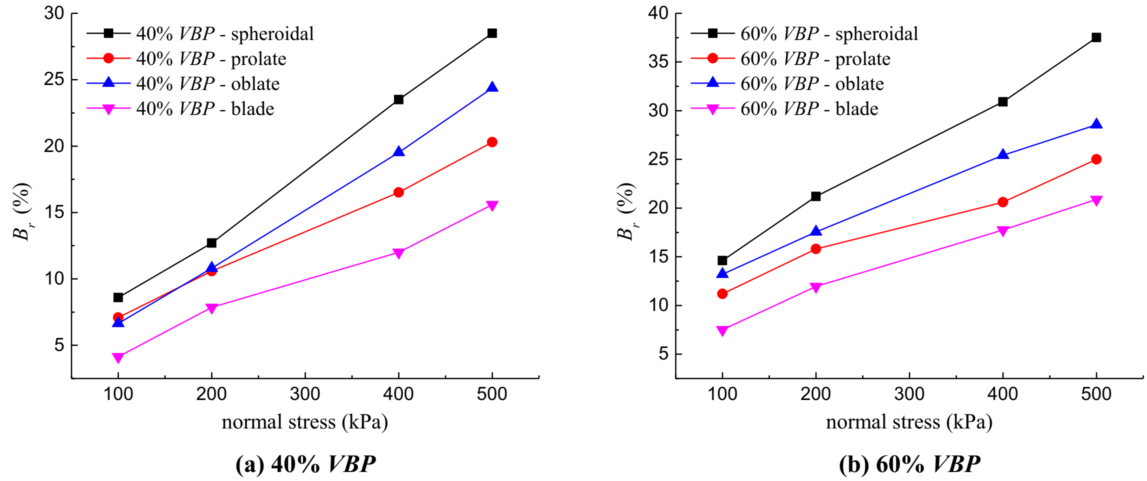

Fig. 15 Meso-ratio of block breakage of soft S–RM samples B_r when the horizontal displacement reaches 56 mm

$$R_a = \frac{\sum_{i=1}^{\text{nstep}} \sum_{\mathrm{j}=1}^{N_{\text{block}}} r_{i,j}^{\text{block}}}{N_{\text{block}}}, \tag{11}$$

where the $r_{i,j}^{block}$ is the rotation magnitude of jth block in ith time step. It is defined as:

$$r_{i,j}^{\text{block}} = \left(\frac{\sum_{\mathrm{m}=1}^{N_{\text{non - break}}} r_m^{\text{ball}}}{N_{\text{non - break}}} \right)_{i,j}, \tag{12}$$

where r_m^{ball} is the rotation magnitude of the mth ball in the block, can be obtained by the intrinsic function *ball.euler* in PFC^{3D}; and $N_{\text{non-break}}$ is the number of balls still bonding with the other balls in the block.

A larger value of R_a indicates a larger magnitude of the block rotation in the S–RM sample, as expected occurring for increasing values of the horizontal displacement during the shearing stage of the test (Fig. 14). The 60% *VBP* samples are characterized by lower values of R_a than those with a 40% *VBP*, demonstrating that the increase of block percentage obstructs the block rotation during the shearing.

The block form was found to have a different influence on the block rotation under different normal stresses. For low σ_n, the R_a values of samples with spheroidal, prolate and oblate blocks are similar and higher than those with blade blocks. Differently, for high σ_n, maximum values of R_a were obtained in the case of spheroidal and oblate blocks, followed by the prolate and blade ones. This fact indicates that blade blocks have more difficulties in rotating in the S–RM sample in comparison to the other block forms, while the rotation of spheroidal and oblate blocks is in general easier. Rotation of prolate blocks is more facilitated under low σ_n. These phenomena are more pronounced when the *VBP* is high.

5.1.4 Block Breakage Characteristics

The meso-ratio of block breakage B_r is used for quantitatively evaluating the block breakage degree in the S–RM samples during the shearing stage. It is defined as follows:

$$\mathrm{B}_r = \frac{N_{\text{bond - break}}}{N_{\text{bond}}} \times 100\% , \tag{13}$$

where $N_{\text{bond-break}}$ is the total number of broken bonding contacts and N_{bond} is the total number of bonding contacts before the shearing of the samples.

The B_r values of all samples at the end of shearing are summarized in Fig. 15. The B_r of samples with a 40% *VBP* varies between 4 and 27%, while it lies in the range of 7–37% for the 60% *VBP* samples, indicating that the increase in *VBP* promotes the breakage of blocks.

The breakage degree is maximum for the spheroidal blocks, followed by the oblate, prolate and blade ones. The reason is possibly related to the combined influence of the block frictional slide and rotation. In fact: (a) the blade blocks have the smallest B_r in comparison to the other form blocks in relation to the reduced sliding and rotation occurring during the shear stage; (b) the B_r of spheroidal blocks is larger than that of oblate ones, because the interlocking degree and frictional sliding of the former are significantly larger although their rotation magnitude is similar; (c) under high σ_n, the B_r of oblate blocks is larger than that of the prolate ones, because the rotation magnitude of the former is larger although the large amount of frictional sliding of the latter, probably indicating that the rotation of blocks contributes more significantly to the breaking process than the sliding.

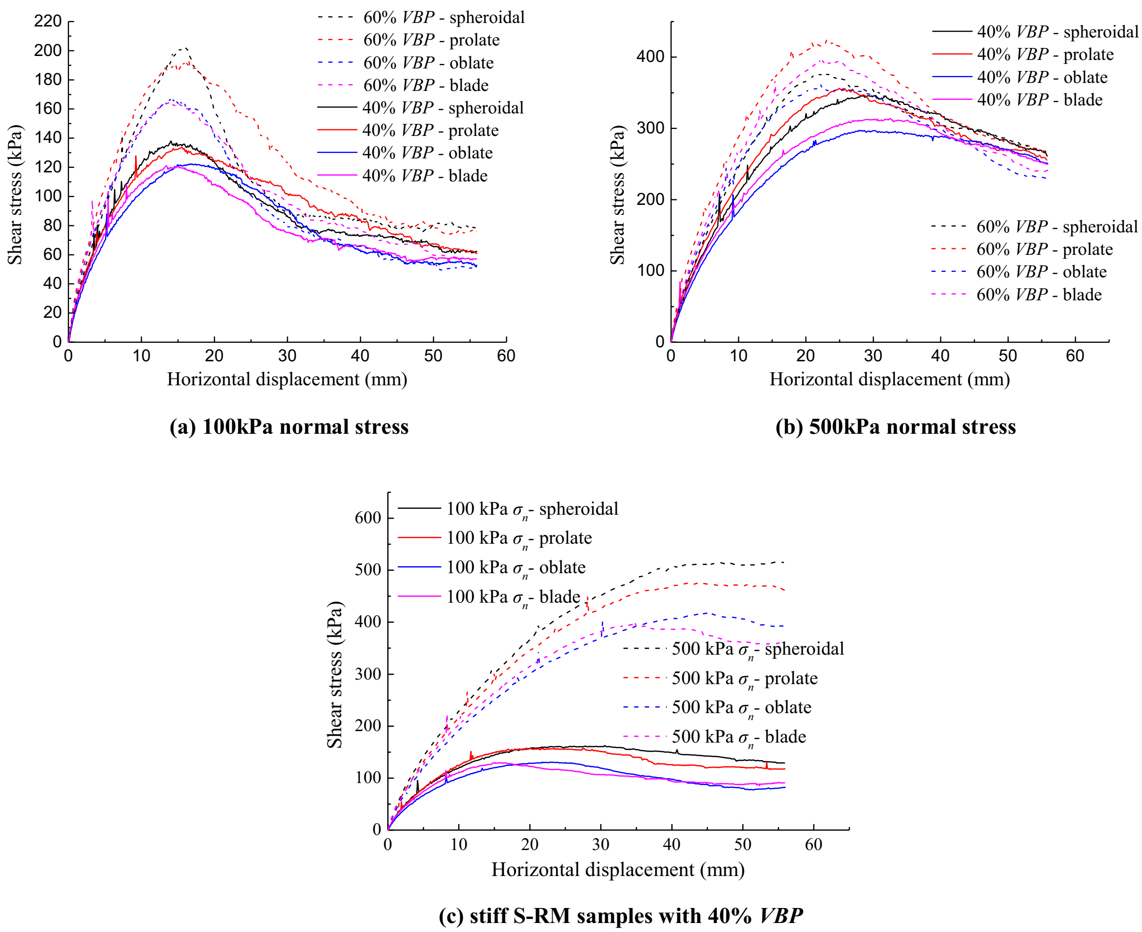

Fig. 16 Shear stress—horizontal displacement curves of the S–RM samples with different block forms

5.2 Macroscopic Behaviour

This paragraph describes the macroscopic behaviour of soft S–RMs with different block forms. To further illustrate the effect of block breakage on the macroscopic mechanical behaviour of soft S–RMs, DEM shear tests without block breakage were also simulated for the sake of comparison, considering different block forms and a 40% *VBP*. These samples, named in the following stiff S–RMs, were generated by simply increasing the bond strength of soft block clusters to 10 GPa.

5.2.1 Shear Strength

As shown in Fig. 16, all soft S–RM samples display a strain-softening behaviour, the shear stress reducing rapidly after reaching the peak value. In contrast, stiff samples show a strain-hardening response when σ_n is 500 kPa (Fig. 16c), indicating that the block breakage plays a fundamental role in the soft S–RM behaviour.

In terms of block form, the peak strength is always larger for the spheroidal block samples under 100 kPa σ_n, followed by the prolate, then oblate and blade forms. In general, the effect of block forms on the peak strength is more apparent for larger *VBP*. This result is explained by considering that the peak strength is mainly controlled by the interlocking degree of blocks and the breakage degree of blocks. As such, the peak strength of samples with spheroidal and prolate blocks are larger due to their more intense interlocking degree, being the influence of block breakage very limited when the σ_n is low.

A different evidence is found for the tests with $\sigma_n = 500$ kPa for the soft S–RMs. Soft samples with a 40% *VBP* are characterized by the highest peak strength in the case of prolate blocks, followed by the spheroidal, blade and oblate ones. In the 60% *VBP* samples, the order is modified into prolate, blade, spheroidal and oblate blocks. This phenomenon is due to the larger number of block breakage occurring during the shearing stage under high σ_n, leading to a larger reduction in the strength, especially for the spheroidal and oblate blocks characterized

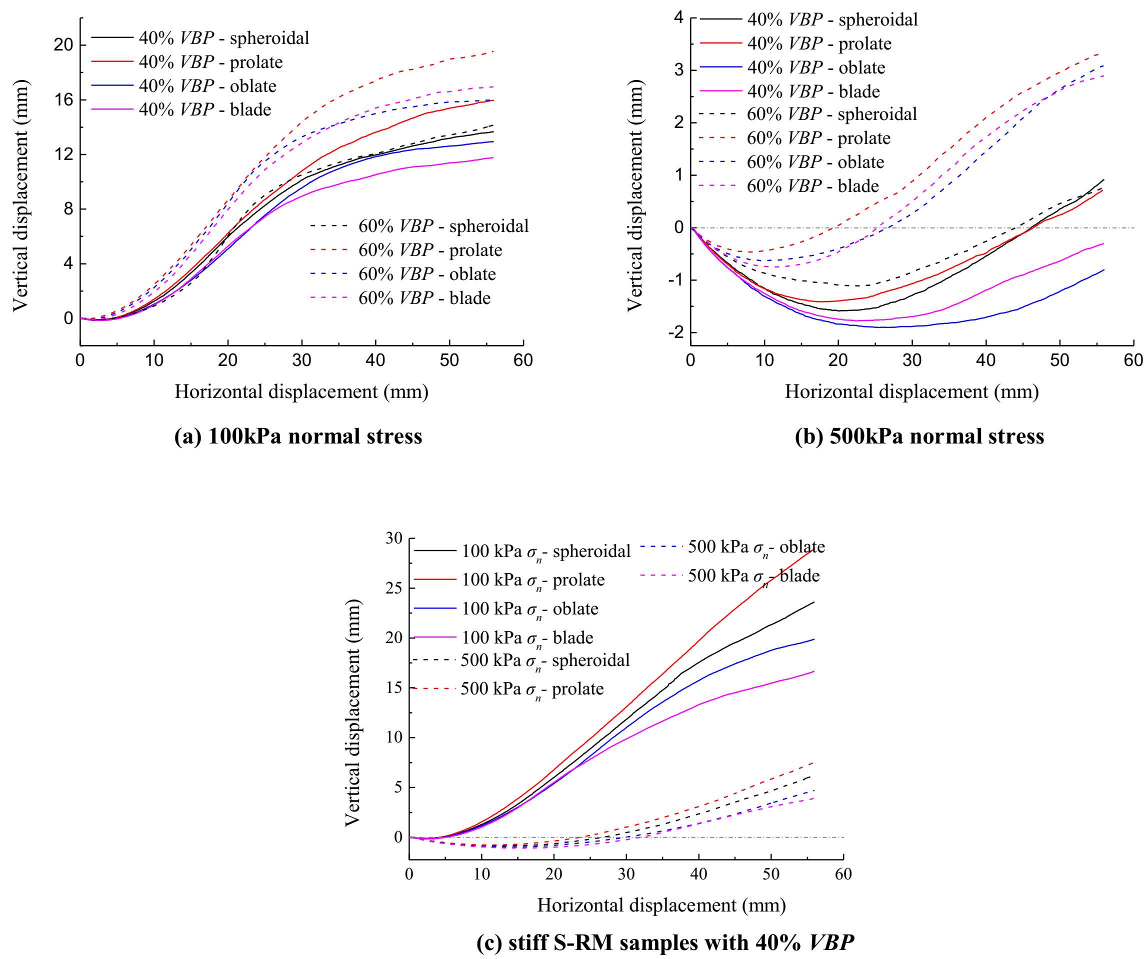

Fig. 17 Vertical displacement—horizontal displacement curves of the S–RM samples with different block forms

by the larger breakage degree. The larger reduction in peak strength occurs in the samples with the higher *VBP*, because of the corresponding increment in the block breakage degree.

Stiff samples, independently on the applied normal stress, always display a larger strength in the case of spheroidal blocks, followed by the prolate, blade and oblate ones, demonstrating that the effect of block form on the soft S–RM behaviour is largely controlled by block breakage phenomena.

5.2.2 Shear Dilation

Figure 17 illustrates the vertical versus horizontal displacement curves obtained during the shearing of S–RM samples. Compared to stiff S–RMs, samples with breakable blocks have a limited dilatative response. The response under lower σ_n is dominated by dilation, while the pattern changes from contraction to dilation for the higher σ_n.

For the soft samples with spheroidal blocks, the change of *VBP* has a little influence on the dilation of the samples; in contrast, the increase in *VBP* in the samples having other block forms produces a clear increase in the dilatative tendency.

Except for the spheroidal blocks, the prolate blocks are associated to the more intense dilatative response during shearing, followed by the oblate and blade blocks.

5.2.3 Shear Strength Parameters

As highlighted in other researches (Tu et al. 2021; Sonmez et al. 2021), the strength envelope of S–RM samples, especially containing breakable blocks, is typically non-linear. As such, an improved non-linear Mohr–Coulomb strength criterion (N-MC criterion) was adopted. It is characterized by a friction angle φ decreasing with σ_n according to the following expression:

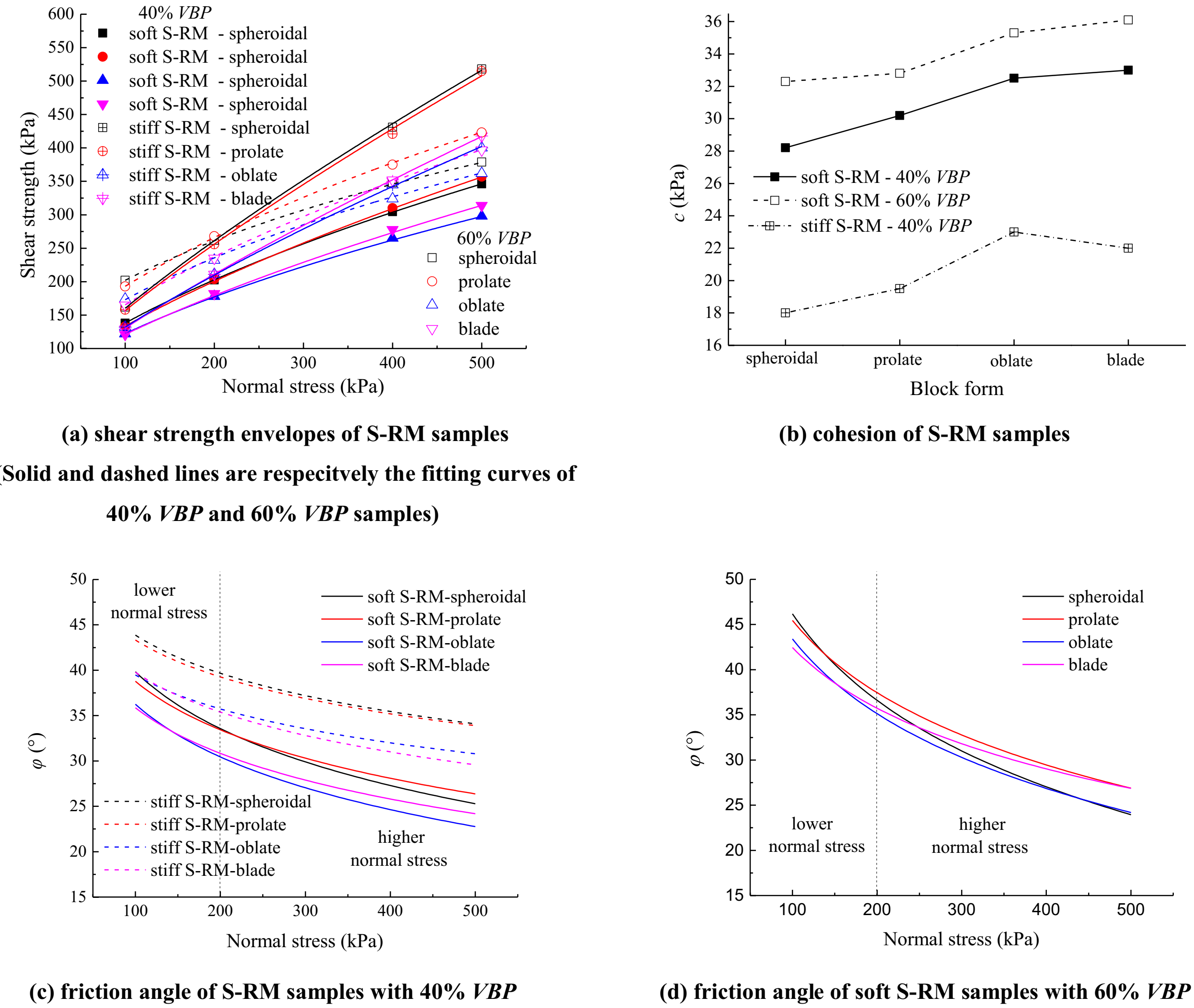

(a) shear strength envelopes of S-RM samples (Solid and dashed lines are respecitvely the fitting curves of 40% *VBP* and 60% *VBP* samples)

(b) cohesion of S-RM samples

(c) friction angle of S-RM samples with 40% *VBP*

(d) friction angle of soft S-RM samples with 60% *VBP*

Fig. 18 Shear strength envelopes and shear strength parameters of the S–RM samples with different block forms

Table 5 Initial and non-linear friction angle of S–RM samples with different block forms

Block form	φ_0 (°)			$\Delta\varphi$ (°)			R^2		
	Soft S–RM		Stiff S–RM	Soft S–RM		Stiff S–RM	Soft S–RM		Stiff S-RM
	40% *VBP*	60% *VBP*	40% *VBP*	40% *VBP*	60% *VBP*	40% *VBP*	40% *VBP*	60% *VBP*	40% *VBP*
Spheroidal	39.7	46.0	43.8	20.8	31.9	14.0	0.996	0.992	0.988
Prolate	38.7	45.3	43.3	17.8	26.6	13.5	0.996	0.982	0.985
Oblate	36.1	43.3	39.4	19.3	27.5	12.4	0.985	0.990	0.979
Blade	35.8	42.3	39.7	16.7	22.3	14.6	0.981	0.991	0.976

$$\varphi = \varphi_0 - \Delta\varphi \lg\left(\frac{\sigma_n}{P_a}\right), \quad (14)$$

where φ_0 is the initial friction angle and P_a is the standard atmospheric pressure, equal to 101.3 kPa. $\Delta\varphi$ represents the φ reduction magnitude with the increase of σ_n.

The resulting N-MC criterion is thus expressed as follows:

$$\tau = c + \sigma_n \times \tan\left(\varphi_0 - \Delta\varphi \lg\left(\frac{\sigma_n}{P_a}\right)\right), \quad (15)$$

where c is the cohesion of samples.

As shown in Fig. 18a, the adopted relationship fits very well the peak strength values, the R^2 of fitting curves being all larger than 0.97. This demonstrates that the N-MC criterion is more appropriate for describing the mechanical behaviour of S-RMs than the linear one, especially for soft S-RMs.

As summarized in Table 5, stiff S–RMs have larger φ_0 and smaller $\Delta\varphi$ than the soft ones, indicating that the block breakage reduces the friction resistance and increases the reduction magnitude of strength with increasing σ_n. For the soft S–RMs, the samples with spheroidal and prolate blocks require higher values of φ_0 than those with oblate and blade blocks, due to their larger frictional resistance. Larger values of $\Delta\varphi$ are expected for spheroidal and oblate blocks in comparison to prolate and blade ones, owing to their larger block breakage degree. The increase in *VBP* not only is associated to a higher value of $\Delta\varphi$, but is also characterized by the more evident influence of the block form.

The strength parameters of soft S–RM samples with different block forms are shown in Fig. 18. The cohesion c of soft S–RMs is larger than that characterizing the stiff samples. And the c of soft S–RMs displays an increase for increasing *VBP* values and is significantly affected by the block forms. The S–RM sample has a higher c when it contains blade and oblate blocks, while lower values were found in the case of spheroidal and prolate blocks.

The friction angle φ of stiff S–RMs is larger than that of soft ones, obviously indicating that the block breakage reduces the frictional resistance of S–RMs. In the soft samples with 40% *VBP*, the φ of soft S–RMs with spheroidal and prolate blocks is larger than that with blade and oblate blocks, given the larger interlocking of spheroidal and prolate blocks. However, for the samples with 60% *VBP* and the higher normal stress, the samples with prolate and blade blocks have the largest φ values in comparison to the spheroidal and oblate ones, in relation to the larger block breakage degree of the spheroidal and oblate ones. The *VBP* was found to have a larger influence on the friction angle φ of the soft S–RMs in the lower normal stress range than in the higher one.

6 Conclusions

In this paper, a novel 3D geometry modelling approach for the generation of stochastic block geometries with different forms but same convexity and angularity was proposed using spherical harmonics series of CT scanned blocks. An already existing non-overlapping DEM modelling approach was also improved for accurately representing the morphology of 3D blocks and their possible block breakage with a reduced computational cost. Numerical direct shear tests were performed on the generated 40% *VBP* and 60% *VBP* soft S–RM DEM samples with different block forms. The meso- and macro- shear behaviours of all samples were analyzed in detail for investigating the influence of the block form. The main conclusions are summarized as follows.

Considering the mesoscopic behaviour, the interlocking degree of blocks, associated to the frictional resistance, is largest for the spheroidal form, followed by the prolate, oblate and blade ones, especially when the *VBP* is high. The block rotation magnitude of samples with spheroidal, prolate and oblate blocks is similar and larger than that observed in the case of blade blocks under low normal stress; under high normal stress it becomes larger for samples with spheroidal and oblate blocks, more pronounced when the *VBP* is high. The breakage degree is maximum for the spheroidal blocks, followed by the oblate, prolate and blade ones, due to the possible combined influence of the block frictional slide and, especially, rotation.

For the macroscopic behaviour, it was found that, as expected, the block breakage reduces the shear strength and is associated to a more evident strain-softening response in the post-peak regime. Under low normal stress, the largest shear strength is obtained for spheroidal block samples, due to the higher interlocking degree of blocks and the limited influence of block breakage at this stress level. In contrast, the maximum strength is observed for soft samples containing prolate and blade blocks, due the larger number of blocks broken in the spheroidal and oblate block samples under high normal stress.

It was found that the non-linear criterion is more appropriate for describing the shear strength envelope of S–RMs than the linear one, especially for soft S–RMs. The block breakage increases the cohesion c, while reducing the friction angle. The soft S–RM sample is characterized by a higher c if containing blade and oblate blocks. The friction angle φ of soft S–RMs with spheroidal and prolate blocks, due to their larger frictional resistance, is higher than that with blade and oblate blocks when *VBP* is 40%. For samples with 60% *VBP* subjected to the higher normal stress, reduced values of φ are observed for spheroidal and oblate block samples due to their larger block breakage degree. The *VBP* is significantly affecting the φ of the soft S–RMs under low normal stresses while it reduces its importance when the applied normal stress is higher.

For the soft S–RM artificial slope in the southwestern China, that inspired this study, the optimum characteristics are a 60% of *VBP* and the use of prolate blocks. For slope height in the range 8–22 m, the friction angle is typically between 29° and 40°. In general, useful indications for the design of S–RM artificial slopes containing breakable soft blocks are that a higher friction angle is reached if spheroidal and prolate blocks are selected when the *VBP* is 40%, while prolate and blade blocks need to be used under higher normal stress when *VBP* is 60%.

Acknowledgements This study is funded by the Yalong River Joint Fund (No. U1965109) and High Speed Rail Joint Fund (No. U2034203).

References

Ai J, Chen JF, Rotter JM, Jin YO (2011) Assessment of rolling resistance models in discrete element simulations. Powder Technol 206:269–282

Calseira LMMS, Brito A (2014) Use of soil-rock mixtures in dam construction. J Constr Eng Manag 140(8):04014030

Cen D, Huang D, Ren F (2017) Shear deformation and strength of the interphase between the soil-rock mixture and the benched bedrock slope surface. Acta Geotech 12(2):391–413

Christoph S, Luis FP, Torsten W (2021) Numerical analyses of the 2D bearing capacity of block-in-matrix soils (bimsoils) under shallow foundations. Comput Geotech 136:104232

Coli N, Berry P, Boldini D (2011) In situ non-conventional shear tests for the mechanical characterisation of a bimrock. Int J Rock Mech Min Sci 48(1):95–102

Coli N, Boldini D, Bandini A, Lopes DS (2012) Modeling of complex geological rock mixtures under triaxial testing conditions. In: ISRM International Symposium - EUROCK 2012, Stockholm, Sweden, May 2012. International Society for Rock Mechanics and Rock Engineering. Paper Number: ISRM-EUROCK-2012-108

Ferellec JF, McDowell GR (2010) A method to model realistic particle shape and inertia in DEM. Granular Matter 12(5):459–467

Graziani A, Rossini C, Rotonda T (2012) Characterization and DEM modeling of shear zones at a large dam foundation. Int J Geomech 12(6):648–664

Hamidi A, Azini E, Masoudi B (2012) Impact of gradation on the shear strength—dilation behavior of well graded sand-gravel mixtures. Scientia Iranica 19(3):393–402

He ZL, Zhang JY, Sun T (2020) Influence of maximum particle diameter on the mechanical behavior of soil-rock mixtures. Adv Civ Eng 3:8850221

Hu XL, Zhang H, Boldini D, Liu C, He CC, Wu SS (2021) 3D modelling of soil-rock mixtures considering the morphology and fracture characteristics of breakable blocks. Comput Geotech 132:103985

Hu XL, Zhang H, He CC, Zheng WB (2018) Breakage effect of soft rock blocks in soil-rock mixture with different block proportions. In: Wu W, Yu HS. (eds) Proceedings of China-Europe Conference on Geotechnical Engineering. Springer Series in Geomechanics and Geoengineering. Springer, Cham, pp. 809–813. https://doi.org/10.1007/978-3-319-97112-4_181

Jin L, Zeng YW, Zhang S (2017a) Large scale triaxial tests on effects of rock block proportion and shape on mechanical properties of cemented soil-rock mixture. Rock Soil Mech 38(1):141–149

Jin L, Zeng YW, Ye Y, Li JJ (2017b) Improving three-dimensional DEM modeling methods for irregularly shaped particles and their assembly. Chin J Geotech Eng 39(7):1273–1281

Kahraman S, Alber M, Fener M, Gunaydin O (2015) An assessment on the indirect determination of the volumetric block proportion of Misis fault breccia (Adana, Turkey). Bull Eng Geol Env 74(3):899–907

Kalender A, Sonmez H, Medley EW, Tunusluoglu C, Kasapoglu KE (2014) An approach to predicting the overall strengths of unwelded bimrocks and bimsoils. Eng Geol 183:65–79

Khorasani E, Amini M, Hossaini MF, Medley EW (2019) Evaluating the effects of the inclinations of rock blocks on the stability of bimrock slopes. Geomech Eng 17(3):281–287

Li X, Liao QL, He JM (2004) In-situ tests and a stochastic structural model of rock and soil aggregate in the three gorges reservoir area, China. Int J Rock Mech Min Sci 41(3):702–707

Li Y, Huang R, Chan LS, Chen J (2013) Effects of particle shape on shear strength of clay-gravel mixture. KSCE J Civ Eng 17(4):712–717

Li Z, Hu F, Qi S, Hu R (2020) Strain-softening failure mode after the post-peak as a unique mechanism of ruptures in a frozen soil-rock mixture. Eng Geol 274:105725

Lindquist ES (1994) The strength and deformation properties of mélange. Dissertation, University of California.

Liu XR, Tu YL, Wang P, Zhong ZL, Tang WB, Du LB (2017) Particle breakage of soil-rock aggregate based on large-scale direct shear tests. Chin J Geotech Eng 39(8):1425–1434

Liu FF, Mao XS, Fan YS, Wu LP, Liu WV (2020) Effects of initial particle gradation and rock content on crushing behaviors of weathered phyllite fills—a case of eastern Ankang section of Shiyan—Tianshui highway, China. J Rock Mech Geotech Eng 12(2):269–278

Medley EW, Rehermann PFS (2004) Characterization of bimrocks (rock/soil mixtures) with application to slope stability problems. In: Proceedings of EUROCK 2004 & 53rd Geomechanics Colloquium Salzburg. pp 425–430

Medley EW (1994) The engineering characterization of mélanges and similar block-in-matrix rocks (bimrocks). Dissertation, University of California.

Meng QX, Wang HL, Cai M, Xu WY, Zhuang XY (2020) Three-dimensional mesoscale computational modeling of soil-rock mixtures with concave particles. Eng Geol 277:105802

Minuto D, Morandi L (2015) Geotechnical characterization and slope stability of a relict landslide in bimsoils (blocks in matrix soils) in dowtown Genoa, Italy. Eng Geol Soc Territory Landslide Process 2:1083–1088

Napoli ML, Barbero M, Ravera E, Scavia C (2018a) A stochastic approach to slope stability analysis in bimrocks. Int J Rock Mech Min Sci 101:41–49

Napoli ML, Barbero M, Scavia C (2021) Tunneling in heterogeneous rock masses with a block-in-matrix fabric. Int J Rock Mech Min Sci 138:104655

Napoli ML, Barbero M, Scavia C (2018b) Analyzing slope stability in bimrocks by means of a stochastic approach. In: Geomechanics and Geodynamics of Rock Masses—European Rock Mechanics Symposium, EUROCK 2018. pp 427–433

Napoli ML, Barbero M, Scavia C (2019) Slope stability in heterogeneous rock masses with a block-in-matrix fabric. In: Rock Mechanics for Natural Resources and Infrastructure

Development- Proceedings of the 14th International Congress on Rock Mechanics and Rock Engineering, ISRM 2019. pp 3482–3489.
Nie ZH, Fang CF, Gong J, Liang ZY (2020) DEM study on the effect of roundness on the shear behaviour of granular materials. Comput Geotech 121:103457
Roadifer JM, Forrest MP (2012) Characterization and treatment of mélange and sandstone foundation at Calaveras dam. In: Proceedings of Geo Congress 2012 State of the Art and Practice in Geotechnical Engineering. pp 3362–3371
Sonmez H, Gokceoglu C, Medley EW, Tuncay E, Nefeslioglu HA (2006) Estimating the uniaxial compressive strength of a volcanic bimrock. Int J Rock Mech Min Sci 43(4):554–561
Sonmez H, Medley E, Kalender A, Dagdeleneler G, Ozcan NT, Ercanoglu M (2021) An empirical method for predicting the strength of bim materials using modifications of Lindquist's and Leps' approaches. Challenges and Innovations in Geomechanics. Proceedings of the 16th International Conference of IACMAG. pp 759–767
Tu YL, Chai HJ, Liu XR, Wang JB, Zeng B, Fu X, Yu JY (2021) An experimental investigation on the particle breakage and strength properties of soil-rock mixture. Arab J Geosci 14:840
Wang HL, Sha C, Xu WY, Meng QX (2020a) Research on strength of soil-rock mixture based on particle discrete element method. Chin Civil Eng J 53(9):106–114
Wang S, Li Y, Gao X, Xue Q, Wu Z (2020b) Influence of volumetric block proportion on mechanical properties of virtual soil-rock mixtures. Eng Geol 278(1):105850
Wei HZ, Xu WJ, Xu XF, Meng QS, Wei CF (2018) Mechanical properties of strongly weathered rock-soil mixtures with different rock block contents. Int J Geomech 18(5):0401802
Xu WJ, Zhang HY (2021) Research on the effect of rock content and sample size on the strength behavior of soil-rock mixture. Bull Eng Geol Env 80(3):2715–2726
Xu WJ, Hu RL, Tan RJ (2007) Some geomechanical properties of soil-rock mixtures in the Hutiao Gorge area, China. Géotechnique 57(3):255–264
Xu WJ, Xu Q, Hu RL (2011) Study on the shear strength of soil-rock mixture by large scale direct shear test. Int J Rock Mech Min Sci 48(8):1235–1247
Xu WJ, Wang S, Zhang HY, Zhang ZL (2016) Discrete element modelling of a soil-rock mixture used in an embankment dam. Int J Rock Mech Min Sci 86:141–156
Xu WJ (2008) Study on meso-structural mechanics (M-SM) characteristics and stability of slope of soil-rock mixtures (S-RM). Dissertation, Institute of Geology and Geophysics, Chinese Academy of Science
Yang YT, Sun YH, Sun GH, Zheng H (2019) Sequential excavation analysis of soil-rock-mixture slopes using an improved numerical manifold method with multiple layers of mathematical cover systems. Eng Geol 261(1):1–13
Zhang HY, Xu WJ, Yu YZ (2016a) Triaxial tests of soil-rock mixtures with different rock block distributions. Soils Found 56(1):44–56
Zhang ZL, Xu WJ, Xia W, Zhang HY (2016b) Large-scale in situ test for mechanical characterization of soil-rock mixture used in an embankment dam. Int J Rock Mech Min Sci 86:317–322
Zhang H, Hu XL, Boldini D, He CC, Liu C, Ai CJ (2020) Evaluation of the shear strength parameters of a compacted S-RM fill using improved 2-D and 3-D limit equilibrium methods. Eng Geol 269:105550
Zhao BD, Wang JF (2016) 3D quantitative shape analysis on form, roundness, and compactness with μCT. Powder Technol 291:262–275
Zhou B, Wang JF, Zhao BD (2015) Micromorphology characterization and reconstruction of sand particles using micro X-ray tomography and spherical harmonics. Eng Geol 184(14):126–137